Chemistry–A European Journal
Research Article
doi.org/10.1002/chem.202301406
Chemistry Europe
European Chemical Societies Publishing
www.chemeurj.org

Special Collection

On the Role of N-Heterocyclic Carbene Salts in Alkyl Radical Generation from Alkyl Alcohols: A Computational Study

Nil Sanosa[+],[a] Diego Ambrosi[+],[a] Pedro Ruiz-Campos,[a] Diego Sampedro,*[a] and Ignacio Funes-Ardoiz*[a]

Dedicated to Professor Pedro J. Campos on the occasion of his retirement

Abstract: Formation of carbon-carbon bonds through cross-coupling reactions using readily available substrates, like alcohols, is crucial for modern organic chemistry. Recently, direct alkyl alcohol functionalization has been achieved by the use of N-Heterocyclic Carbene (NHC) salts via in situ formation of an alcohol-NHC adduct and its activation by a photoredox catalyst to generate carbon-centered alkyl radicals. Experimentally, only electron deficient NHC activators work but the reasons of this behavior remain underexplored. Herein, a DFT computational study of the mechanism of alcohol activation using up to seven NHC salts is performed to shed light into the influence of their electronic properties in the alkyl radical formation. This study demonstrates that four reaction steps are involved in the transformation and characterizes how the electronic properties of the NHC salt affect each step. A fine balance of the NHC electron-richness is proved to be determinant for this transformation.

Introduction

Modern-day chemical synthesis is supported by carbon-carbon bond formation as one of the key reactions in organic chemistry.[1] The relevance of this transformation is clearly supported by the uninterrupted exploitation of known approaches and the proliferation of new and improved methodologies.[2] This has allowed the direct assemble of organic fragments to yield a wide range of substrates. As such, cross-coupling reactions are still the most reliable and reproducible methodology for C–C and C-heteroatom bond formation,[3] taking advantage of a plethora of carbon scaffolds as versatile building blocks to prepare high-value compounds.[4] In addition, the advent of photoredox catalysis as a reliable and straightforward strategy to generate open-shell intermediates under mild conditions has increased the ability to generate a variety of carbon-centered radicals as coupling partners.[5] Thus, sp^3-based substrates have become prominent precursors for cross-coupling transformations[6] and hence, they can be used as a reliable carbon source for state-of-the-art chemical synthesis.[7]

Despite of the notable advances that have been reached in different types of cross-coupling reactions,[8] the development of new and versatile coupling partners continues to be a topic of interest.[9] This has been usually performed through the gradual incorporation of commercially available substrates in cross-coupling reactions.[10] Since the initial discoveries in cross-coupling in the early 1970s by Kumanda, Kochi, Corriu and Murahashi,[11] many different organic electrophiles have been successfully employed in these transformations. Initially, organo iodides/bromides were broadly used due to their high reactivity.

However, the development of modern catalytic systems has paved the way for the introduction of alternative and less reactive cross-coupling electrophiles. For instance, aryl chlorides[12] as well as fluorides[13] were first reported, followed by O-containing organic compounds including alkenyl/arenyl triflates,[14] sulfonates[15] and phosphonates.[16] Despite of the noteworthy development in Pd-catalyzed cross-coupling of C–O electrophiles,[17] the direct C–O activation of O-based electrophiles remained challenging due to the inert character of the C–O bond. This was a critical drawback of this reactivity as a wide variety of esters, ethers and alcohols that are abundantly produced in industrial applications could not be used in these transformations. Clearly, with new methodologies, these substrates could become powerful cross-coupling electrophiles, especially alcohols, which perfectly match the criteria to be used in these reactions due to their high synthetic versatility,

[a] N. Sanosa,[+] D. Ambrosi,[+] P. Ruiz-Campos, Dr. D. Sampedro, Dr. I. Funes-Ardoiz
Department of Chemistry,
Centro de Investigación en Síntesis Química (CISQ),
Universidad de La Rioja
C/ Madre de Dios 53, 26004 Logroño (Spain).
E-mail: diego.sampedro@unirioja.es
Ignacio.funesa@unirioja.es

[+] These authors contributed equally to this work

Supporting information for this article is available on the WWW under https://doi.org/10.1002/chem.202301406

Special Collection This manuscript is part of a joint special collection on Mechanisms and Selectivities of Organic Reactions – In Celebration of Prof. Kendall N. Houk's 80th birthday.

low price and large abundance. Indeed, alcohols have been already included in some similar reactions even if they require pre-functionalization steps.[18] This led to a situation in which, even if the use of alcohols in cross-coupling reactions was greatly desirable, their direct activation remained mainly under-explored.

This challenge was addressed by MacMillan and co-workers, by reporting an unprecedented dual (Ir/Ni) catalytic strategy for the C_{sp^2}–C_{sp^3} bond-formation using commercially available alcohols (Figure 1, B).[19] This innovative metal-catalyzed cross-coupling procedure was a starting point for a new type of synthetic procedures that greatly increased the range of C–C bond-forming transformations. This represented a significant advance in cross-coupling methods since previously the alcohol substrate required a pre-activation step and did not tolerate a great number of alkyl substrates.[20] The direct activation of alcohols allowed for the introduction of common N-heterocyclic carbene (NHC) salts[21] (Figure 1, A). In these reactions, NHC salts act as an effective C_{sp^3}–OH activating agent that enables a unique direct deoxygenative coupling using primary, secondary and tertiary alcohols in one pot. Since then, a number of new strategies using NHC salts such as deoxyfluorination of alcohols[22] as well as C_{sp^3}–C_{sp^3} cross-coupling of alcohols and carboxylic acids[23] have recently appeared (Figure 1, A).

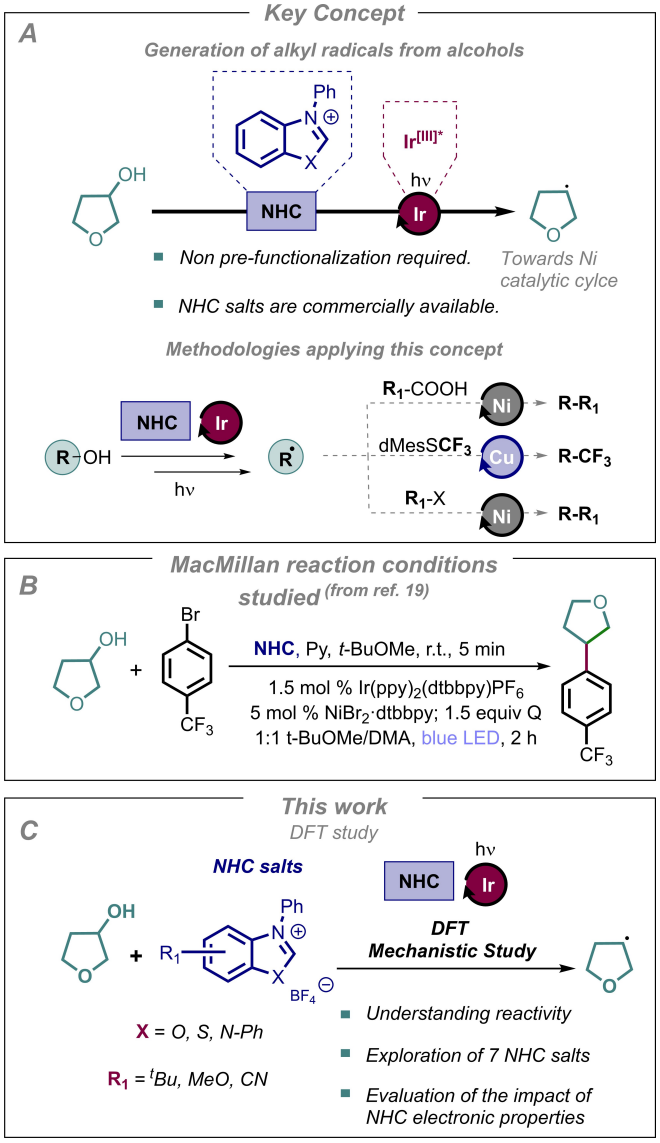

Figure 1. Generation of C-centered radicals from NHC-alcohol adducts (A). Experimental conditions for deoxygenative arylation of alcohols (B). This work: DFT study of alkyl radical generation from alcohols of seven distinct NHC salts (C).

Over the past decades, density-functional theory (DFT) calculations have been employed to unveil mechanistic insight into reactions involving transition-metal-catalytic systems.[24] This methodology allows to obtain the guiding principles for such reactions aimed at understanding the underlying mechanisms as well as at improving the reaction efficiency. Under this scenario and taken into account our interest in photoredox catalysis reactivity during the last years,[25] we aimed to comprehensively study the mechanism of the photoredox-mediated alcohol-NHC activation (Figure 1, B), exploring systematically up to seven different NHC salts to understand the effect of the electronic properties in the kinetic and thermodynamic profile of the reaction.

Herein, we present a DFT computational study for the evaluation of the influence of NHC on the carbon radical generation from NHC-alcohol adducts, that then undergoes Ni-catalyzed arylation reactivity (Figure 1, C). We focused on the radical generation step which is the one influenced by the nature of the NHC salt.

Results and Discussion

The proposed reaction mechanism is depicted in Figure 2, A. First, the alcohol undergoes a nucleophilic attack on the most electrophilic carbon of the NHC salt forming an adduct and releasing one proton to the pyridine, which acts as a base. Then, this intermediate can be oxidized by the [Ir^{III}] photocatalyst, as demonstrated by Stern-Volmer quenching experiments. The oxidized radical cation increased the acidity of the NHC proton that can be again deprotonated by the base to form the unstable carbon radical, surrounded by three heteroatoms. Finally, this intermediate can evolve through a β-scission to form the stable aromatized carbamate and the carbon-centered alkyl radical. It was also proved that only very electron deficient NHC salts worked in this transformation and was hypothesized that the reason was the stable adduct formation (Figure 2, B). In order to shed light on the different steps of the reaction, we have explored the detailed mechanism of this transformation by means of Density Functional Theory calculations (see Supporting Information for computational details)[26] to unravel the key parameters that favors the reactivity of NHCs. We aim to analyze the influence of the electronic properties of different NHCs in all the steps of the reaction mechanism and we will show that the electron richness affects differently in every elementary step of the mechanism.

To obtain further insight into the operational mechanism of the NHC adduct formation, we first examined the full mecha-

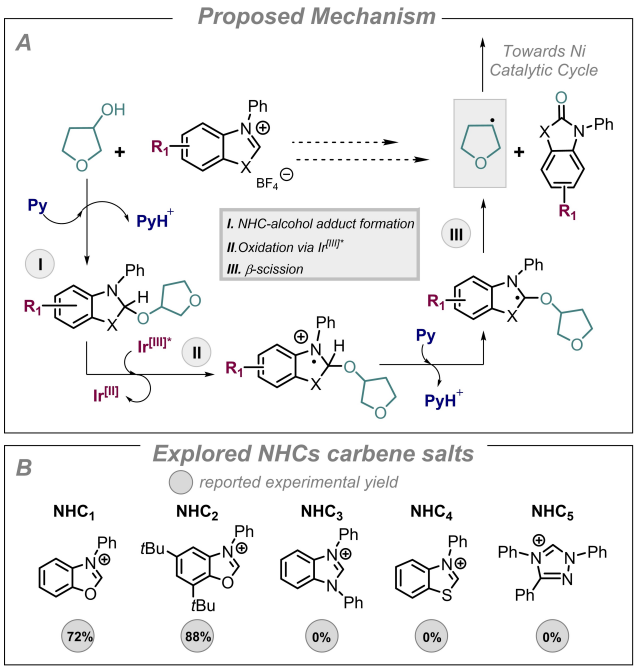

Figure 2. Proposed mechanism for alkyl radical formation from alcohols (A). Set of NHCs carbene salts employed by MacMillan and also used in this study (B).

nism of **NHC$_1$**, which shows a good experimental performance (Figure 3). The mechanism starts with the concerted nucleophilic attack of the alcohol to the electrophilic NHC imine moiety through **TS1** with a low barrier of 19.1 kcal/mol, likely due to the stabilizing π-π stacking interactions that can appear between the pyridine and the aromatic ring. This allows the concerted deprotonation by the pyridine due to the aromatic ring spatial position in which the nitrogen of the pyridine abstracts the hydrogen of the alkyl alcohol (R–OH) at a distance of only 1.07 Å. We also explored the step-wise process but the direct deprotonation of the alcohol by the pyridine base to form **8** was found prohibitively energetic (43.1 kcal/mol) making this pathway clearly unfavorable. After intermediate **3** is generated, the excited Ir-photocatalyst is able to oxidize this species affording the α-amino radical **4** (−0.6 kcal/mol). Although we did not calculate the electron transfer barrier, we assume a low barrier based on related metal-based photoredox catalytic systems.[25a] This cationic intermediate is formed through a slightly endergonic process (ΔG_{SET} = 2.1 kcal/mol). The α-hydrogen atom is now more acidic due to the proximity to the positive charge and the electro-withdrawing environment caused by both the oxygen and nitrogen neighboring atoms.

In the next step, pyridine acts as a base to abstract this acidic α-hydrogen atom reaching **TS2** (16.1 kcal/mol).[27] Once intermediate **5** is formed, it rapidly progresses into a carbamate via β-scission as a by-product **6** and yields the required desoxygenative alkyl radical **7** in a highly exergonic process due to the C=O formation. More specifically, looking at the C–O distances of **5**, **TS3** and **7**, we noticed how the single C–O bond (1.34 Å in **5**) is shortened in **TS3** (1.25 Å) to finally become a double bond in **7** (1.20 Å), being this transformation the driving force of the process. In this way, the carbon-centered radical can be accessed exergonically (ΔG° = −28.5 kcal/mol) based on a four step-reaction: formation of NHC activated alcohol, SET, deprotonation and β-scission.

With this mechanistic picture in mind, we next sought to explore the energy profiles of the set of other 4 NHC salts that had been tested experimentally. Also, as a computational experiment, we slightly modified the *N*-aryl benzoxazolium skeleton introducing –CN and –OMe groups in the phenyl backbone of the good performing N-aryl benzoxazolium salt in order to evaluate the influence of highly donating and highly electron withdrawing groups (**NHC$_6$**, **NHC$_7$**, Figure 4, A).

Therefore, by using these additional NHC salts, we were able to evaluate the impact of the electronic properties in the two extreme cases for each step of the alkyl radical generation process: **NHC$_6$** acts as the most electron donating and **NHC$_7$** as the most electron withdrawing NHC salts employed for this study. A detailed description of the five different kinetic and thermodynamic reaction parameters is provided in Figure 4, B, to understand the large variability of the NHC influence in the reaction outcome. This includes:

- NHC adduct formation thermodynamics (red circle, 1).
- NHC adduct formation kinetics (yellow circle, 2).
- Oxidation of NHC-alcohol adduct by the [Ir^{III}] photocatalyst in the excited state (blue circle, 3)
- Span free energy activation barrier of the whole process (purple circle, 4).[28,29]
- Free energy difference between reactants and products (green circle, 5)

With an operationally computational outline in hand, we next explored the energy profiles for the remaining body of NHCs carbene salts proposed. After analyzing the first transition state values we noticed that, as proposed before, the more electron deficient the NHC salt is, the lower the first activation free energy barrier and the more stabilized the NHC-alcohol adduct will be (Figure 4, B, 1 and 2). For example, the comparison between the electron rich **NHC$_6$** and the electron deficient **NHC$_7$** shows a significant difference in the adduct barrier formation (+7.5 kcal/mol higher for the electron rich **NHC$_6$**). This electronic effect also has a direct impact on the alcohol-adduct stability. Thus, only those NHC adducts generated from electron deficient NHCs can be formed exergonically (**NHC$_1$**, **NHC$_2$** and **NHC$_7$**). However, this stabilization should be moderated as in **NHC$_1$** (−0.4 kcal/mol) and in **NHC$_2$** (−2.0 kcal/mol). Otherwise, a highly stabilized NHC adduct as in **NHC$_7$** (−13.9 kcal/mol) will hamper the next steps of the reaction mechanism. We have also examined the highest barrier of radical generation along all the reaction profiles via the energetic span model (ΔG°_{span}) as a straightforward manner to calculate the catalytic efficiency (See Figure S3 and S4 of the Supporting Information for further details). For those NHC salts sharing a similar core (**NHC$_1$**, **NHC$_2$**, **NHC$_3$** and **NHC$_4$**), the ΔG°_{span} corresponds to the first transition state barrier (18.4, 19.1, 28.1, 21.7 kcal/mol). In the case of NHC$_5$, the ΔG°_{span} (29.7 kcal/mol) is located in the second transition state of the reaction profile,

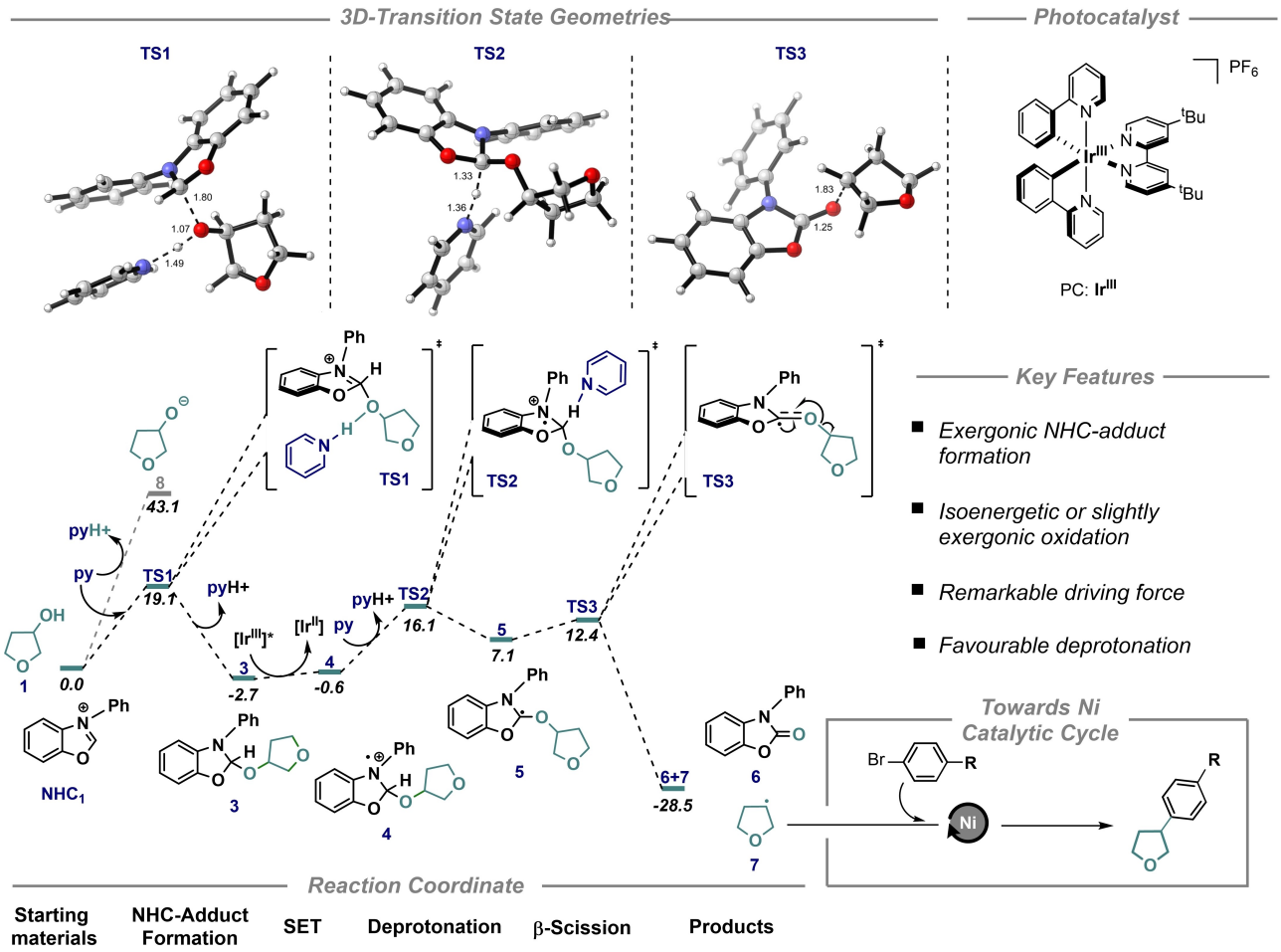

Figure 3. Free energy profile of radical generation via Ir-photoredox cycle. Values in kcal/mol. Bond distances in angstroms.

when the deprotonation step with pyridine takes place. For NHC_6, the overstabilization of the oxidized intermediate and the comparatively higher β-scission implies that the ΔG°_{span} (27.1 kcal/mol) takes place between those two points. Finally, the ΔG°_{span} for **NHC_7** (24.1 kcal/mol) comes from the deprotonation due to the low electron density of the oxidized intermediate.

Then, the Single Electron Transfer step from the [Ir^{III}] excited photocatalyst can only evolve from relatively electron-neutral NHC alcohol adduct like **NHC_1** and **NHC_2**, as observed experimentally. If the system is too electron deficient, like in **NHC_7**, the oxidation is too endergonic (+14.0 kcal/mol) and if the system is too electron rich (**NHC_3**, **NHC_5** and **NHC_6**), the overstabilization of the oxidized adduct considerably increase the free energy span of the whole profile with barriers above 27 kcal/mol. Finally, we found the alkyl radical formation to be exergonic for the whole set of NHC candidates considered. However, we found remarkable differences between some of NHC salts selected (Figure 4 B, 5). Taking into consideration all the commented effects, best results could be achieved with NHC salts with a slightly exergonic NHC adduct formation, followed by a thermodynamically accessible oxidation step. Besides, preparing new NHC salts with substituents leading to very high or very low values of electron density would not be appropriate for the alkyl radical generation.

Conclusion

A comprehensive analysis of the radical generation mechanism from alcohols and NHC salts has been carried out by means of DFT calculations. The results show that this process is divided into four mechanistic steps: a first activation step to form the NHC-adduct, an oxidation step of this adduct via the excited state of Ir(III) photocatalyst, a deprotonation, and a final β-scission to yield the final alkyl radical. The evaluation of different NHC salts stress the effect that the electronic properties of NHC backbone has on reactivity. The ΔG° for the NHC adduct formation increases with more electron deficient NHCs. Conversely, the most electron rich NHC salts feature lower values for ΔG° in the oxidation step. This means that radical generation can be achieved only employing those NHC salts possessing balanced electronic properties, that is, sufficient electron deficiency to facilitate the adduct formation, but enough electron density to undergo oxidation with the photoredox Ir catalyst. We hope this work will help in the develop-

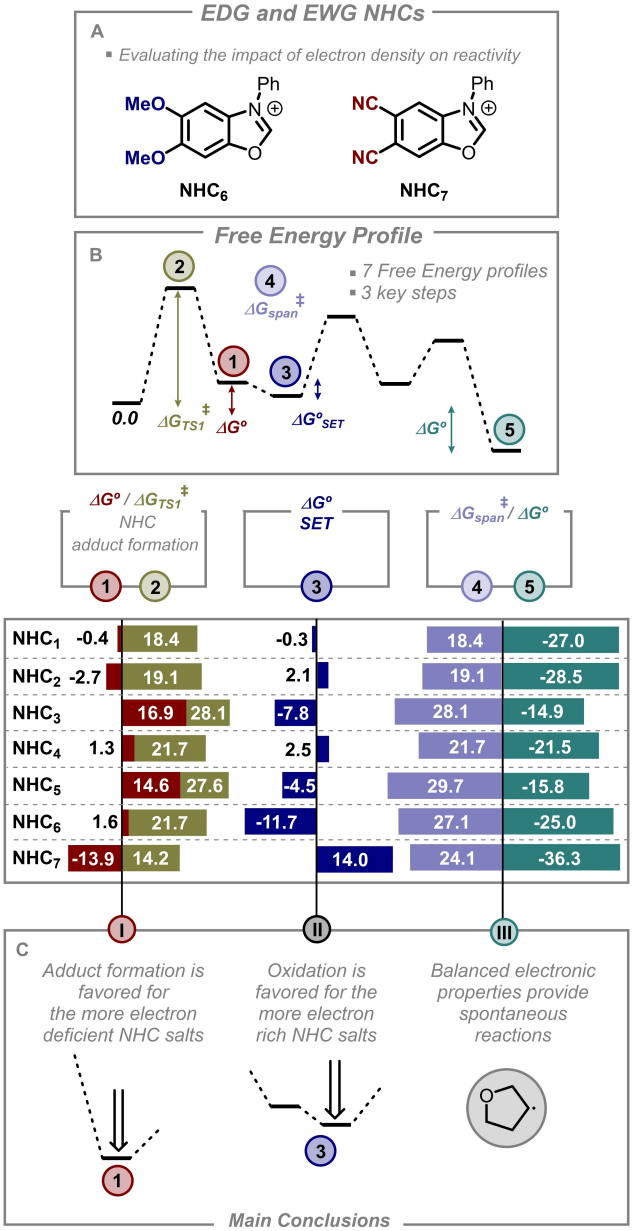

Figure 4. Unexplored NHC salts used in this computational study (A). Simplified reaction profiles of alkyl generation mechanism with NHC salts from NHC_1 to NHC_7 (B). Conclusions drawn from the DFT mechanistic study (C). Values in kcal/mol.

ment challenging alcohol substrate activation and further studies are ongoing in our group to understand the whole catalytic cycle of the transformation.

Computational Method

All Density Functional Theory calculations were carried out using Gaussian 16[30] program package. All the structures were optimized using wB97xD functional combined with the Def2SVP basis set.[31] Besides, a single point calculation employing M06 functional [32] and Def2TZVPP basis set were performed to further refine the potential energies.[24a] Parameters for thermal correction were obtained from the frequency calculation. Solvation was included in both optimizations and single point calculations using the SMD implicit solvent (n.n-Dimethyl Acetamide) model.[33] 3D structures were illustrated using the CYLview 1.0 program.[34]

Supporting Information

Supporting Information is available from the Wiley Online Library.

Acknowledgements

We thank the financial support for project "PID2021-126075NB–I00" financed by the Spanish MCIN / AEI /10.13039/501100011033 FEDER, UE. We also acknowledge the University of La Rioja for financial support. In addition, we thank the "Beronia" cluster at University of La Rioja for computational resources. I.F.A thanks the "Ministerio de Ciencia e Innovación" for the Juan de la Cierva-Incorporation scholarship (IJC2020-045125-I).

Conflict of Interests

The authors declare no conflict of interest.

Data Availability Statement

The data that support the findings of this study are available in the supplementary material of this article.

Keywords: alcohols · cross-coupling · density functional calculations · N-heterocyclic carbene · photoredox catalysis

[1] D. C. Blakemore, L. Castro, I. Churcher, D. C. Rees, A. W. Thomas, D. M. Wilson, A. Wood, *Nat. Chem.* **2018**, *10*, 383–394.
[2] D. G. Brown, J. Boström, *J. Med. Chem.* **2016**, *59*, 4443–4458.
[3] L. C. Campeau, N. Hazari, *J. Organomet. Chem.* **2019**, *38*, 3–35.
[4] a) J. Choi, G. C. Fu, *Science.* **2017**, *356*, eaaf7230; b) Q. Pan, Y. Ping, W. Kong, *Acc. Chem. Res.* **2023**, DOI: 10.1021/acs.accounts.2c00771.
[5] a) N. A. Romero, D. A. Nicewicz, *Chem. Rev.* **2016**, *116*, 10075–10166; b) T. Constantin, M. Zanini, A. Regni, N. S. Sheikh, F. Juliá, D. Leonori, *Science* **2020**, *367*, 1021–1026.
[6] H. A. Sakai, W. Liu, C. C. Le, D. W. C. MacMillan, *J. Am. Chem. Soc.* **2020**, *142*, 11691–11697.
[7] R. Zhang, G. Li, M. Wismer, P. Vachal, S. L. Colletti, Z.-C. Shi, *ACS Med.* **2018**, *9*, 773–777.
[8] S.-r. Guo, P. S. Kumar, M. Yang, *Adv. Synth. Catal.* **2017**, *359*, 2–25.
[9] E. L. Lucas, E. R. Jarvo, *Nat. Chem. Rev.* **2017**, *1*, 0065.
[10] a) C.-T. Yang, Z.-Q. Zhang, J. Liang, J.-H. Liu, X.-Y. Lu, H.-H. Chen, L. Liu, *J. Am. Chem. Soc.* **2012**, *134*, 11124–11127; b) X. Zhang, D. W. C. MacMillan, *J. Am. Chem. Soc.* **2016**, *138*, 13862–13865; c) C. P. Johnston, R. T. Smith, S. Allmendinger, D. W. C. MacMillan, *Nature* **2016**, *536*, 322–325.
[11] D.-G. Yu, B.-J. Li, Z.-J. Shi, *Acc. Chem. Res.* **2010**, *43*, 1486–1495.
[12] E. A. Onoabedje, U. C. Okoro, *Synth. Commun.* **2019**, *49*, 2117–2146.
[13] H. Amii, K. Uneyama, *Chem. Rev.* **2009**, *109*, 2119–2183.

[14] a) H. A. Duong, Z.-H. Yeow, Y.-L. Tiong, N. H. B. Mohamad Kamal, W. Wu, *J. Org. Chem.* **2019**, *84*, 12686–12691; b) L. K. G. Ackerman, M. M. Lovell, D. J. Weix, *Nature.* **2015**, *524*, 454–457.
[15] S. Ito, Y.-i. Fujiwara, E. Nakamura, M. Nakamura, *Org. Lett.* **2009**, *11*, 4306–4309.
[16] A. L. Hansen, J.-P. Ebran, M. Ahlquist, P.-O. Norrby, T. Skrydstrup, *Angew. Chem. Int. Ed.* **2006**, *45*, 3349–3353.
[17] T. Zhou, M. Szostak, *Catal. Sci. Technol.* **2020**, *10*, 5702–5739.
[18] a) T. Suga, Y. Ukaji, *Org. Lett.* **2018**, *20*, 7846–7850; b) P. Ertl, T. Schuhmann, *J. Nat. Prod.* **2019**, *82*, 1258–1263.
[19] Z. Dong, D. W. C. MacMillan, *Nature* **2021**, *598*, 451–456.
[20] a) X.-G. Jia, P. Guo, J. Duan, X.-Z. Shu, *Chem. Sci.* **2018**, *9*, 640–645; b) P. Guo, K. Wang, W.-J. Jin, H. Xie, L. Qi, X.-Y. Liu, X.-Z. Shu, *J. Am. Chem. Soc.* **2021**, *143*, 513–523; c) Z. Li, W. Sun, X. Wang, L. Li, Y. Zhang, C. Li, *J. Am. Chem. Soc.* **2021**, *143*, 3536–3543.
[21] D. G. Gusev, *Organometallics* **2009**, *28*, 6458–6461.
[22] N. E. Intermaggio, A. Millet, D. L. Davis, D. W. C. MacMillan, *J. Am. Chem. Soc.* **2022**, *144*, 11961–11968.
[23] H. A. Sakai, D. W. C. MacMillan, *J. Am. Chem. Soc.* **2022**, *144*, 6185–6192.
[24] a) T. Sperger, I. A. Sanhueza, I. Kalvet, F. Schoenebeck, *Chem. Rev.* **2015**, *115*, 9532–9586; b) J. N. Harvey, F. Himo, F. Maseras, L. Perrin, *ACS Catal.* **2019**, *9*, 6803–6813; c) I. Funes-Ardoiz, F. Schoenebeck, *Chem* **2020**, *6*, 1904–1913; d) A. Duan, F. Xiao, Y. Lan, L. Niu, *Chem. Soc. Rev.* **2022**, *51*, 9986–10015; e) B. Maity, C. Zhu, H. Yue, L. Huang, M. Harb, Y. Minenkov, M. Rueping, L. Cavallo *J. Am. Chem. Soc.* **2020**, *142*, 16942–16952.
[25] a) A. de Aguirre, I. Funes-Ardoiz, F. Maseras, *Angew. Chem. Int. Ed.* **2019**, *58*, 3898–3902; b) G. Lei, M. Xu, R. Chang, I. Funes-Ardoiz, J. Ye, *J. Am. Chem. Soc.* **2021**, *143*, 11251–11261; c) Q. Shi, M. Xu, R. Chang, D. Ramanathan, B. Peñin, I. Funes-Ardoiz, J. Ye, *Nat. Commun* **2022**, *13*, 4453; d) N. Sanosa, B. Peñín, D. Sampedro, I. Funes-Ardoiz, *Eur. J. Org. Chem.* **2022**, *2022*, e202200420.
[26] All the calculations were carried out using SMD (n,n-Dimethyl Acetamide) M06/Def2TZVPP//ωB97xD/Def2SVPP. M06 functional was used to refine potential energies based on the benchmarking analysis of Ref. [24d]. See the section Computational Details in the Supporting Information for further details.
[27] Experimentally, quinuclidine is used as the base for the second step of the reaction. To avoid modelling mixtures, we keep using pyridine, which is weaker than quinuclidine, so this step will be even more favoured.
[28] S. Kozuch, S. Shaik, *Acc. Chem. Res.* **2011**, *44*, 101–110.
[29] For this purpose, the TOF-determining transition state (TDTS) and the TOF-determining intermediate (TDI) were defined for each energy profile, providing the corresponding $\Delta G^{\ddagger}_{span}$. For all the energy profiles, TDTS appears after the TDI so $\Delta G^{\ddagger}_{span}$ is the energy difference between these two states.
[30] Gaussian 16, Revision C.01, M. J. Frisch, G. W. Trucks, H. B. Schlegel, G. E. Scuseria, M. A. Robb, J. R. Cheeseman, G. Scalmani, V. Barone, G. A. Petersson, H. Nakatsuji, X. Li, M. Caricato, A. V. Marenich, J. Bloino, B. G. Janesko, R. Gomperts, B. Mennucci, H. P. Hratchian, J. V. Ortiz, A. F. Izmaylov, J. L. Sonnenberg, D. Williams-Young, F. Ding, F. Lipparini, F. Egidi, J. Goings, B. Peng, A. Petrone, T. Henderson, D. Ranasinghe, V. G. Zakrzewski, J. Gao, N. Rega, G. Zheng, W. Liang, M. Hada, M. Ehara, K. Toyota, R. Fukuda, J. Hasegawa, M. Ishida, T. Nakajima, Y. Honda, O. Kitao, H. Nakai, T. Vreven, K. Throssell, J. A. Montgomery, Jr., J. E. Peralta, F. Ogliaro, M. J. Bearpark, J. J. Heyd, E. N. Brothers, K. N. Kudin, V. N. Staroverov, T. A. Keith, R. Kobayashi, J. Normand, K. Raghavachari, A. P. Rendell, J. C. Burant, S. S. Iyengar, J. Tomasi, M. Cossi, J. M. Millam, M. Klene, C. Adamo, R. Cammi, J. W. Ochterski, R. L. Martin, K. Morokuma, O. Farkas, J. B. Foresman, D. J. Fox, Gaussian, Inc., Wallingford CT, **2016**.
[31] J.-D. Chai, M. Head-Gordon, *Phys. Chem. Chem. Phys.* **2008**, *10*, 6615–6620.
[32] Y. Zhao, D. G. Truhlar, *Theor. Chem. Acc.* **2008**, *120*, 215–241.
[33] J. Tomasi, B. Mennucci, R. Cammi, *Chem. Rev.* **2005**, *105*, 2999–3094.
[34] C. Y. Legault, *CYLview20*, Université de Sherbrooke, **2020** (http://www.cylview.org).

Manuscript received: May 3, 2023
Accepted manuscript online: May 4, 2023
Version of record online: June 5, 2023